Supplement of The Cryosphere, 17, 2585–2606, 2023
https://doi.org/10.5194/tc-17-2585-2023-supplement

The Cryosphere Open Access EGU

Supplement of

Seasonal variability in Antarctic ice shelf velocities forced by sea surface height variations

Cyrille Mosbeux et al.

Correspondence to: Cyrille Mosbeux (cyrille.mosbeux@univ-grenoble-alpes.fr)

Supplementary Material

Text S1. Ocean models including SSH under ice shelves.

Ocean models that are available for obtaining SSH variability under ice shelves are forced by different atmospheric and open ocean boundary conditions. Four models are based on the Regional Ocean Modeling System (ROMS: Shchepetkin and McWilliams, 2005; Haidvogel et al., 2008), and include sea ice and representation of thermodynamic interactions between floating ice shelves and the ocean. A fifth model uses the Nucleus for European Modelling of the Ocean (NEMO) that also includes a dynamic sea ice component and thermodynamic coupling of ice shelves and the ocean. These models are referred to in this paper as SSH_M, where *M* is either the period covered by the ocean modelling or the name of the model.

(i) SSH_{2002}: Tinto et al. (2019) ran a regional simulation for the Ross Sea, using a 5-km horizontal grid and a 20-year spin-up forced with a repeated annual cycle of atmospheric conditions from the Antarctic Mesoscale Prediction System (Bromwich et al., 2005) for the period September 2001 to September 2002.

(ii) SSH_{2010}: Dinniman et al. (2020) ran a circum-Antarctic simulation on a grid with 5-km horizontal spacing. This simulation used a 7-year spin-up forced by an annual cycle of atmospheric conditions from ERA-Interim reanalysis (Dee et al., 2011) for calendar-year 2010.

(iii) SSH_{2007}: Richter et al. (2022) used a circumpolar configuration with 2-km grid spacing, forced with calendar-year 2007 atmospheric conditions from ERA-Interim reanalysis. The northern ocean boundary conditions were obtained from the ECCO2 ocean state estimate (Menemenlis et al., 2008; Wunsch et al., 2009). The year 2007 was chosen to be representative of mean conditions for the period 1992-2011 This model was designed to estimate present day ice shelf melting and explore the influence of tides.

(iv) $SSH_{MetROMS}$: The MetROMS-ice shelf model reported by Naughten et al. (2018) uses a variable-resolution grid, with spacing of 5 km at the southernmost grounding lines of RIS increasing to 15-20 km at the northern boundary at 30°S. This simulation was initialised with

ocean temperature and salinity from ECCO2, then forced with ERA-Interim atmospheric reanalyses for the period 1992-2016.

(v) SSH_{NEMO}: The NEMO-eORCA025 simulation was provided by P. Mathiot (IGE – University of Grenoble Alpes) as an update to the model described by Mathiot et al. (2017). This model uses a circumpolar grid with a 0.25 degree resolution (and an additional grid refinement on the longitude as latitude increases), resulting in ~3–4 km grid spacing at the RIS grounding line and about 8-9 km at the ice front. The model was forced with atmospheric conditions from the JRA-55 reanalysis (Kobayashi et al., 2015, 2021) for the period 1980-2019. SSH_{NEMO} simulations are run with NEMO 4.0.4. They use the eORCA025 with a horizontal resolution of ¼ of a degree at the equator). The grid is also composed of 121 layers with a resolution varying from 1 m at the surface, ~20 m between 100 and 1000 m and increasing to 250 m at about 5000 m. It uses a z* vertical coordinate system that allows a better representation of ice shelf melting, treating it as a mass flux (Mathiot et al., 2017). The ice shelf drafts and bathymetry are from BedMachine v2 (Morlighem et al., 2020). An iceberg calving rate is imposed following Rignot et al. (2013).

To compare the observed and model SSH variations, we calculated time series of spatially-averaged SSH from the five ocean models and the altimetry product for three Ross Sea regions: the deep Ross Sea (DRS), open continental shelf (OCS) and RIS. We used the 1500 m isobath, located on the upper continental slope, to separate the DRS and OCS (see **Fig. 1**). The upper slope is the approximate location of the Antarctic Slope Front that separates offshore circumpolar waters from shelf-modified water masses in the Ross Sea (Orsi and Wiederwohl, 2009).

Table S1. Summary of the different models used to force the ice sheet/shelf model.

Name	Author / Publication	Model	Covered Area	Period
SSH_{2002}	Tinto et al. (2019)	ROMS	Ross Sea Regional	2001 – 2002
SSH_{2007}	Richter et al. (2020)	ROMS	Circum-Antarctic	2007 – 2008
SSH_{2010}	Dinniman et al. (2020)	ROMS	Circum-Antarctic	2010 – 2011
$SSH_{MetROMS}$	Naughten et al. (2018)	ROMS	Circum-Antarctic	1992 – 2016
SSH_{NEMO}	Mathiot et al. (pers. comm.)	NEMO	Circum-Antarctic	1980 – 2019

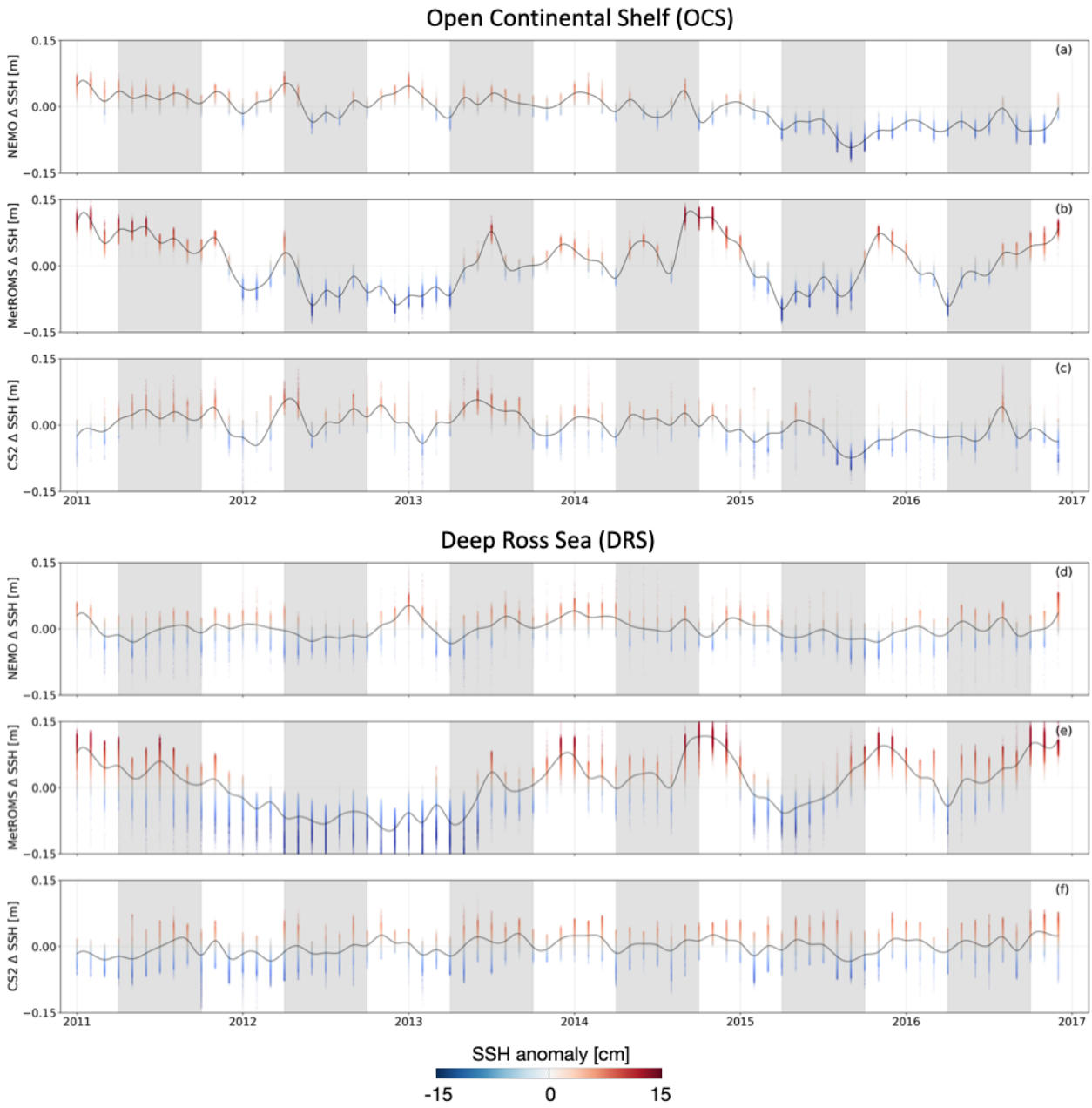

Figure S1. Time series of ΔSSH for the period 2011–2016 over the open continental shelf (see **Fig. 1**) in front of Ross Ice Shelf for (a) NEMO, (b) MetROMS, and (c) CryoSat-2. (d-f) Same ΔSSH but for the deep Ross Sea. Each colored dot represents a 10 x10 km grid cell over the two regions and the grey line represents the averaged value of these cells. The grey shade shows the autumn–winter periods.

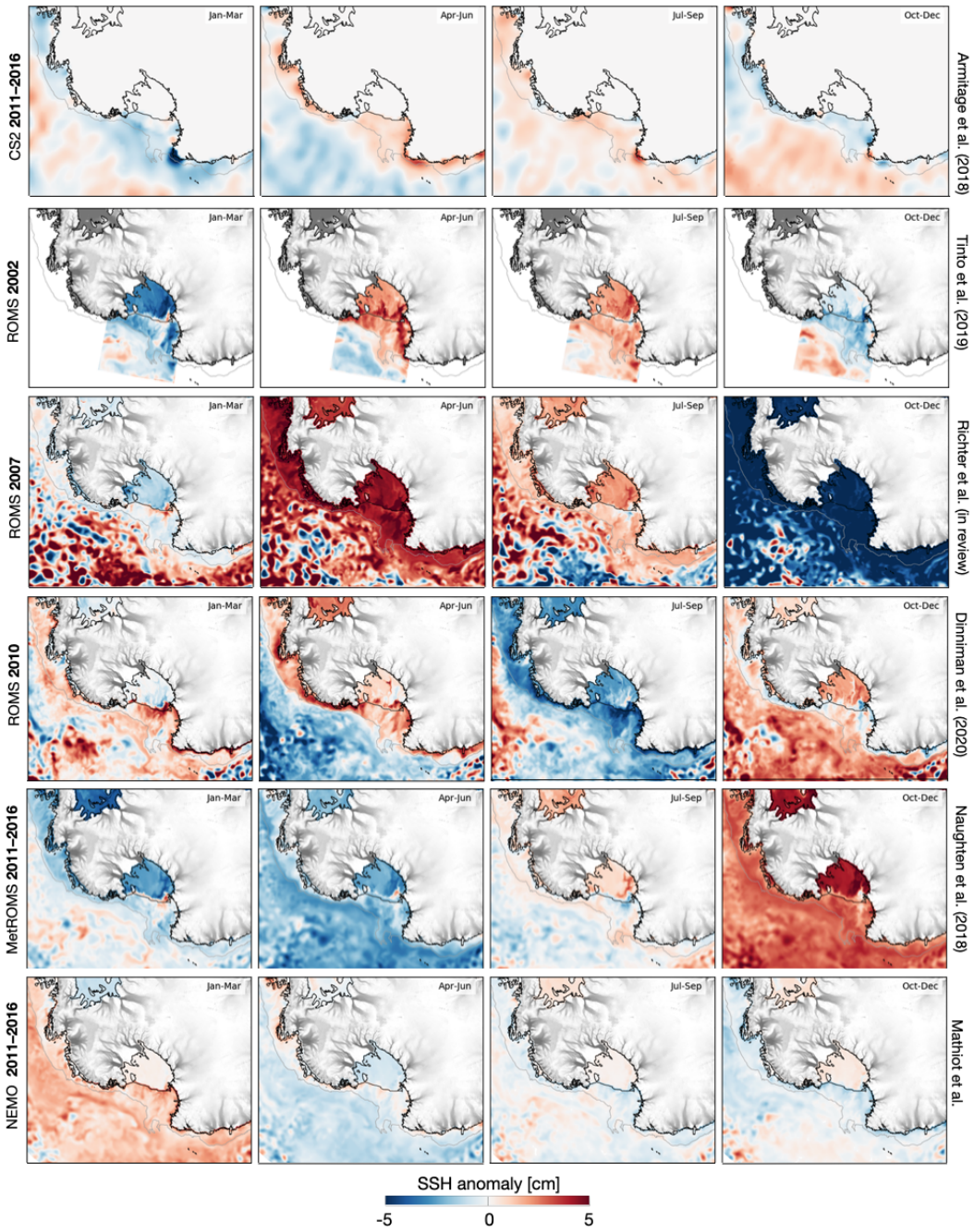

Figure S2. Seasonal deviation of sea surface height (ΔSSH) from the annual mean: (top row) satellite-based observations (Armitage et al., 2018) and (second–sixth row) model outputs for five different models. Ice front and grounding line are represented by black lines. The 1500 m isobath, defining the outer edge of the open continental shelf, is shown by a grey line. Ice surface velocities are plotted on the grounded ice (fast flow in shades of grey).

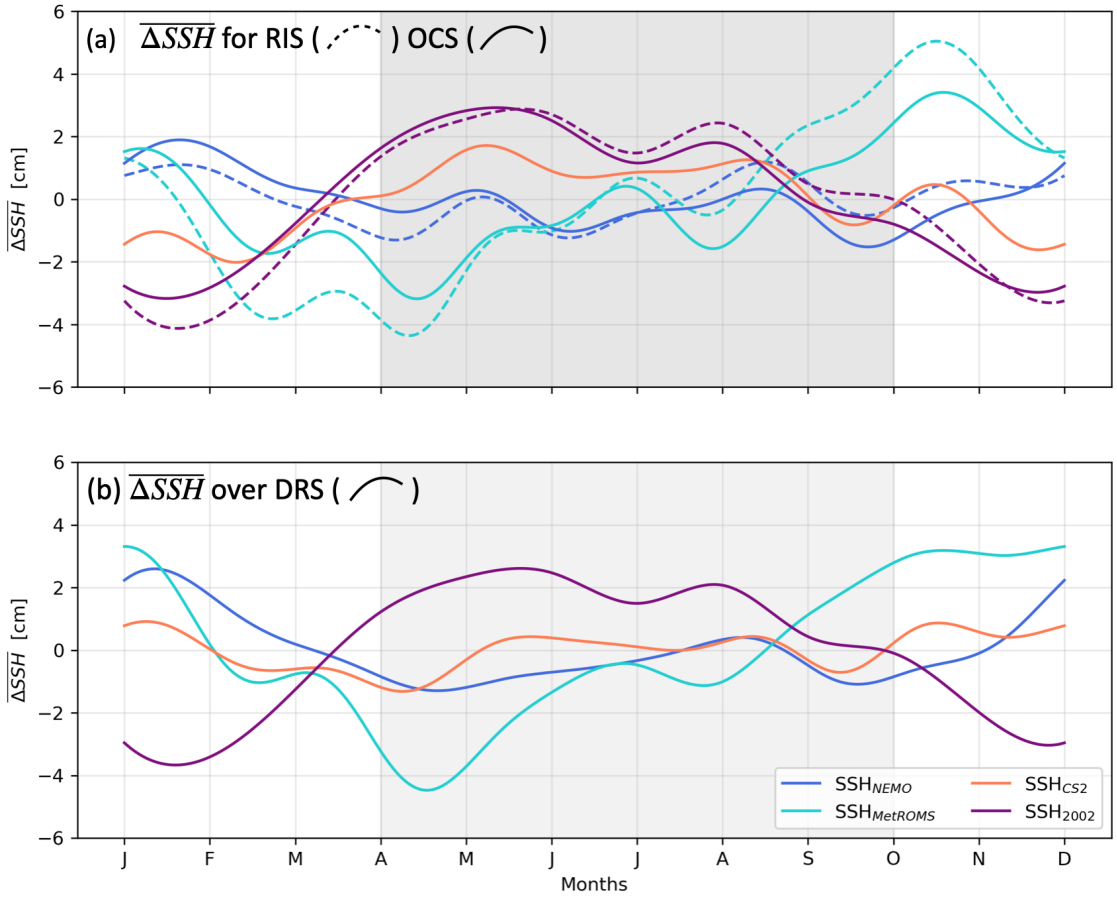

Figure S3. (a) Annual cycle of monthly mean ΔSSH over the open continental shelf (OCS – plain lines) and beneath the ice shelf (RIS – dotted lines) for SSH_{2002}, and for SSH_{NEMO}, $SSH_{MetROMS}$ and SSH_{CS2} averaged over 2011-2016, for the OCS only. (b) Mean ΔSSH for the deep Ross Sea. The grey shade shows the autumn–winter period.

Table S2. P-Correlation between the different models and CryoSat-2 Observations. The P-Correlation is calculated on a 10 km × 10 km resolution grid.

	SSH_{2002}	SSH_{2007}	SSH_{2010}	$SSH_{MetROMS}$	SSH_{NEMO}
Continental Shelf	0.94	0.75	0.63	0.49	0.41
Deep Ocean	0.61	0.72	0.77	0.41	0.47

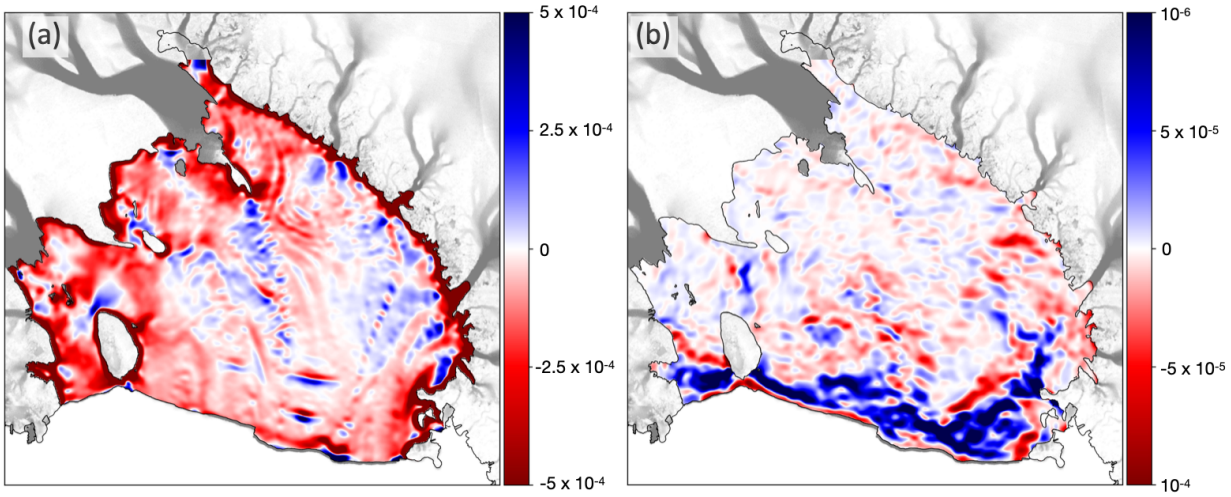

Figure S4. (a) Along-flow gradient of ice shelf surface: red areas experience positive driving stresses (negative slope in the flow direction $\hat{u}$) with a tendency to speed up the ice flow, and blue areas experience negative driving stresses (positive slope along $\hat{u}$) with a tendency to slow down the ice flow. (b) Gradient of ΔSSH in the direction of the flow ($\hat{u}$) in February.

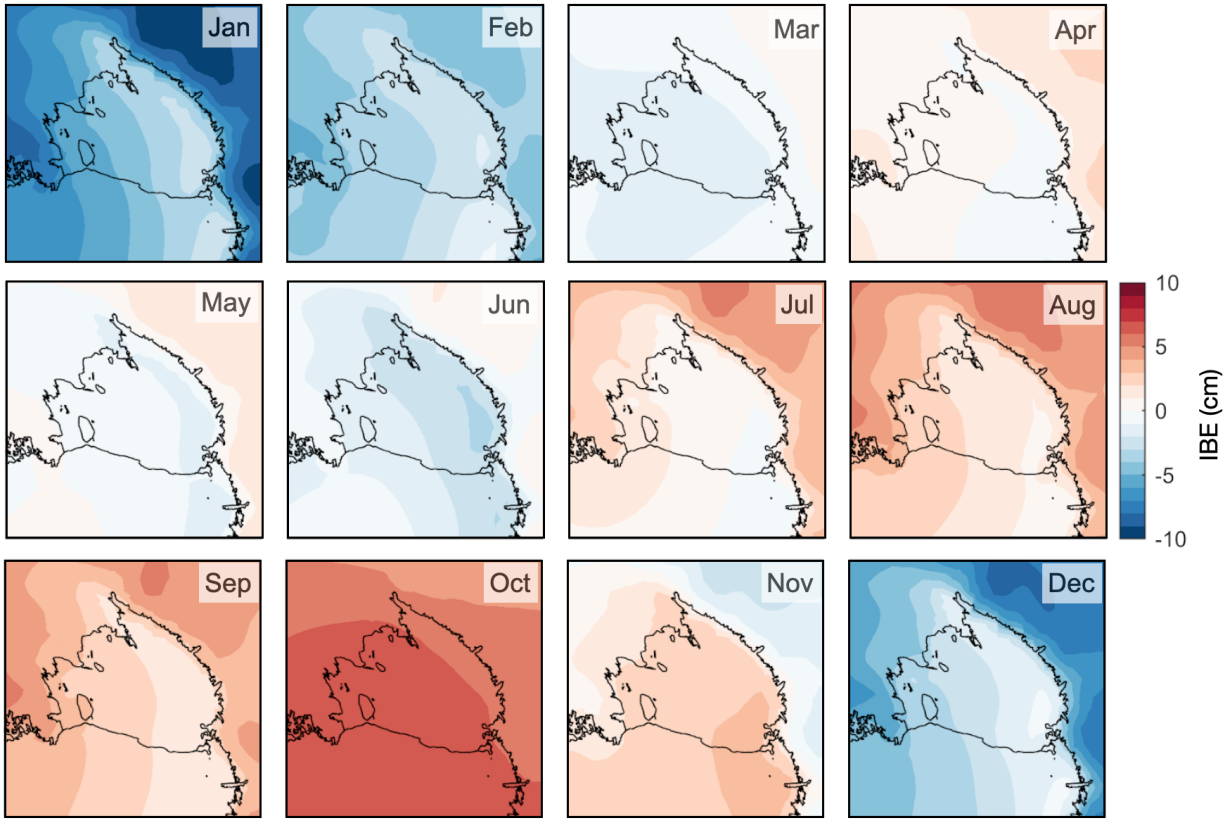

Figure S5. 38-year (1980-2018) monthly average inverse barometer effect over the region of the Ross Ice Shelf, evaluated as -1 cm of SSH change per +1 hPa of surface atmospheric pressure obtained from ERA-Interim (Dee et al., 2011).

Text S2. SSH inter-model variability

We have shown that estimates of ΔSSH are sensitive to the choice of ocean model (see Fig. S1, S2) and that small changes in ΔSSH can have large effects on the modelled ice flow anomaly by modifying both the driving stress through SSH spatial gradients and the grounding line migration (see Sec. 3.3). We forced the ensemble of initial states, with the ΔL_{B2L} parameterisation, with models of ΔSSH_{2002}, ΔSSH_{2007} and ΔSSH_{2010} (**Fig. S6**). As these ocean models do not span the same period of the GNSS time series, we will only investigate the potential of the modelled annual cycle of ΔSSH to affect the ice flow, regardless of the year. However, the difference in

the implementation of the different models and the year of the modelling provides guidance on possible inter-annual variability.

The most extreme difference from one model to another is found when they show an opposite sign of ΔSSH. The model SSH_{2010} predicts $\Delta SSH < 0$ in July–September whereas SSH_{2002} and SSH_{2007} both predict values > 0, leading to an opposite velocity anomaly over the same period. This leads to a poor correlation between velocity anomalies when forcing the ice flow model with $\Delta SSH_{2010}$with respect to ΔSSH_{2002} and ΔSSH_{2007}.

Models SSH_{2002} and SSH_{2007}, which share a similar seasonal pattern of SSH variation, also show a good correlation between their velocity anomalies. For GNSS sites DR10, BATG and LORG, SSH_{2002} shows a good fit to observations over the first part of the year with a minimum velocity anomaly in February. This model then predicts a slower but longer acceleration, leading to a maximum velocity in August (compared to July in the observations); see **Fig. S6a,c,d**). At DR10, SSH_{2007} leads to a minimum and maximum velocity anomaly about one month earlier than in the observations (**Figure S6**). This difference between the two models may come from their different simulation years. Overall, models forced with ΔSSH_{2002} and ΔSSH_{2007} fit the observations at these three GNSS stations, with the envelope obtained by combining the two models including a significant part of the observations.

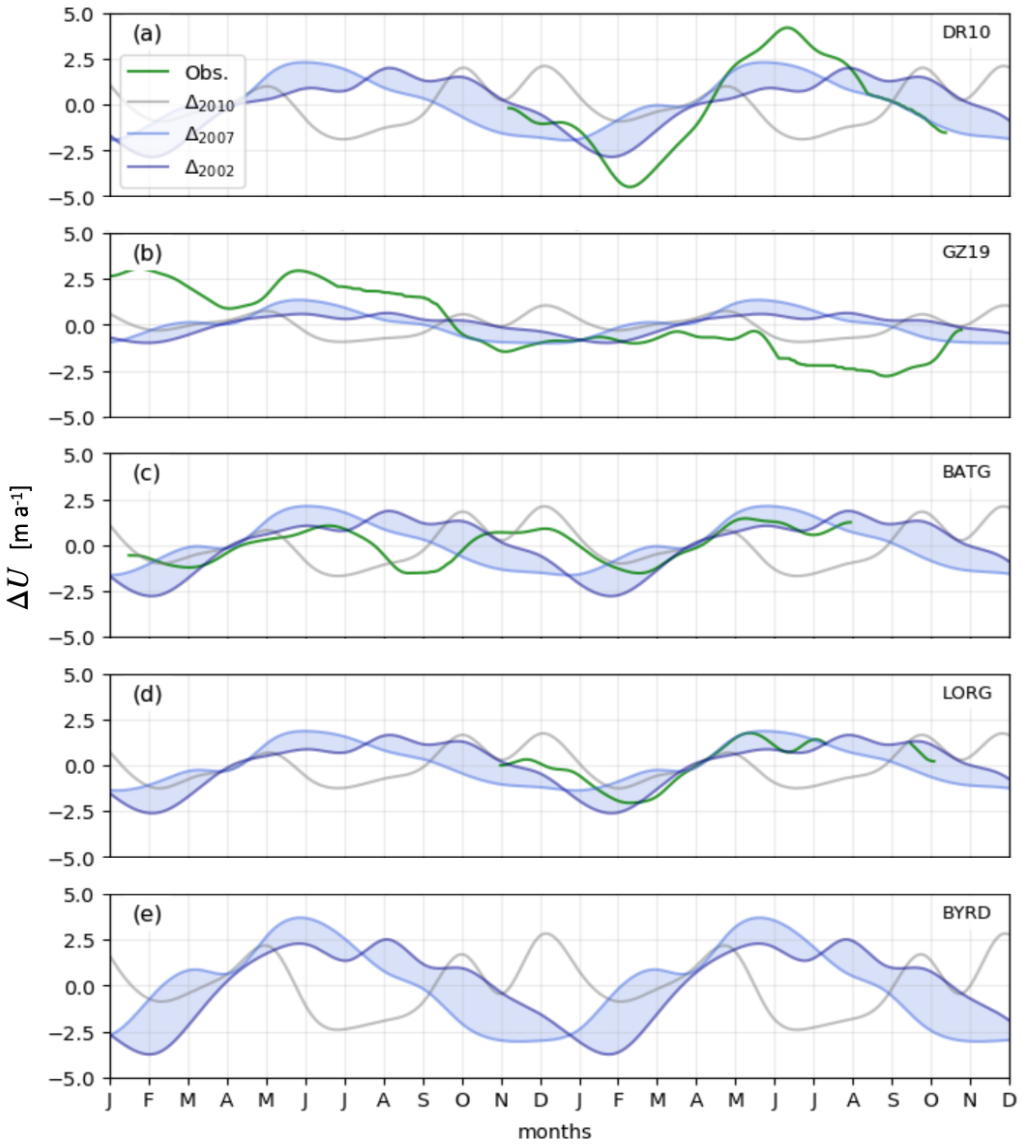

Figure S5. Comparison between GNSS and model velocity anomalies for (a) DR10, (b) GZ19, (c) BATG, and (d) LORG, and (e) at Byrd Glacier outlet (see locations on **Fig. 1**) for the ΔL_{B2L} grounding line migration parameterisation. Only model results are shown for Byrd, since no long-term GNSS data are available there. The model cycle is repeated over 2 years to encompass observations. The average model velocity ΔU_{B2L} (over Ω_{15}) is shown for different SSH forcings from models run with repeated annual cycles: ΔSSH_{2002} (dark blue), ΔSSH_{2007} (light blue) and ΔSSH_{2010} (grey). The light blue shade represents the envelope of velocity anomalies between ΔSSH_{2002} and ΔSSH_{2007}. The observed velocities (green) are the same as in **Fig. 8**.

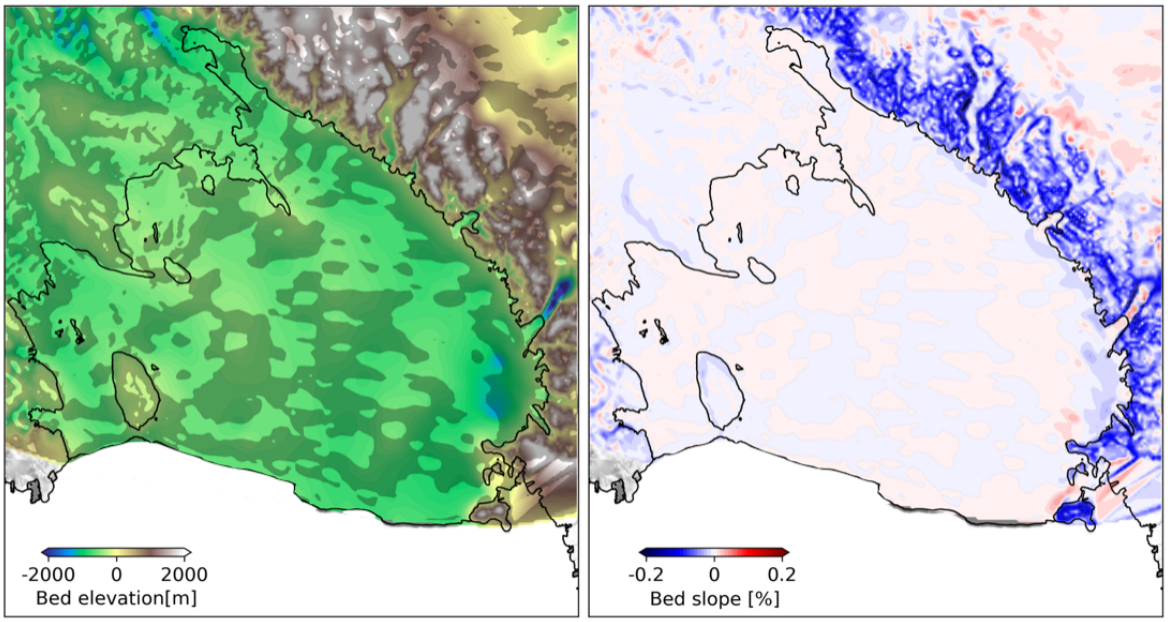

130

Figure S6. (a) Bed elevation with highlighted retrograde slope (sloping upward in the flow direction). (b) Grade (blue) and retrograde (red) bed slope in percentage (%). The mapping is based on the Bedmap2 dataset by Fretwell et al., (2013) and the direction of the ice flow computed during the initialisation phase.

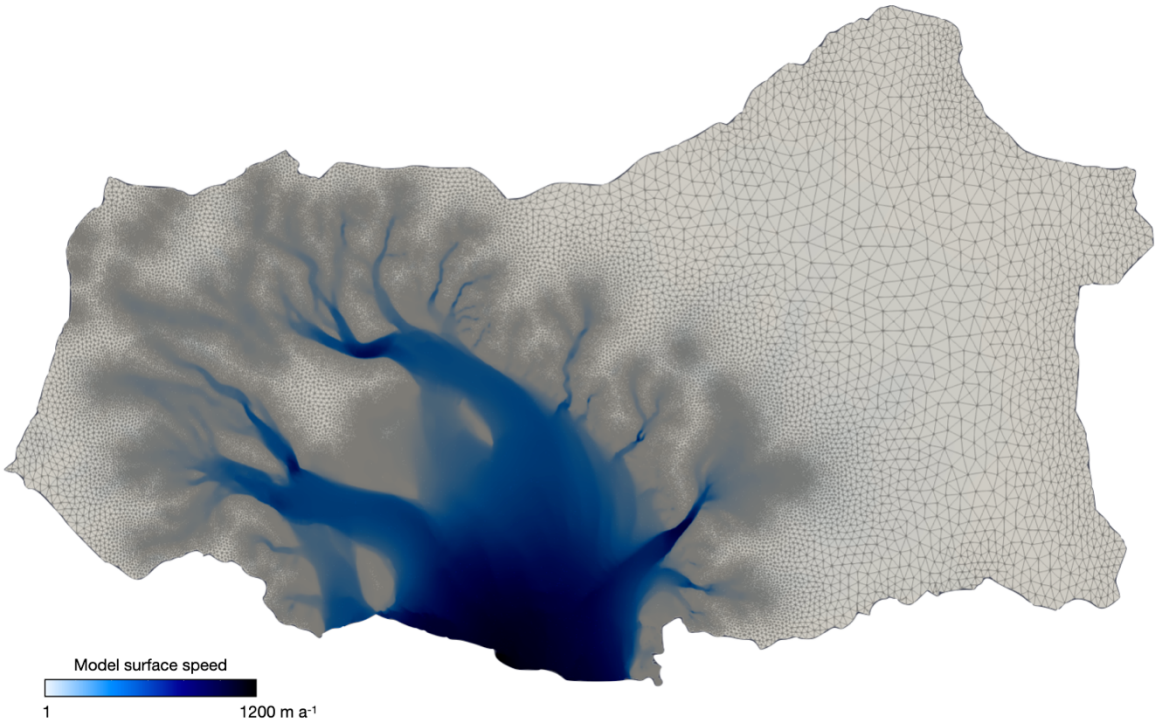

135

Figure S7. Finite Element mesh over the domain used for this study. The resolution varies from 25 km inland to 2 km over the ice shelf, and 500 m at the grounding line.

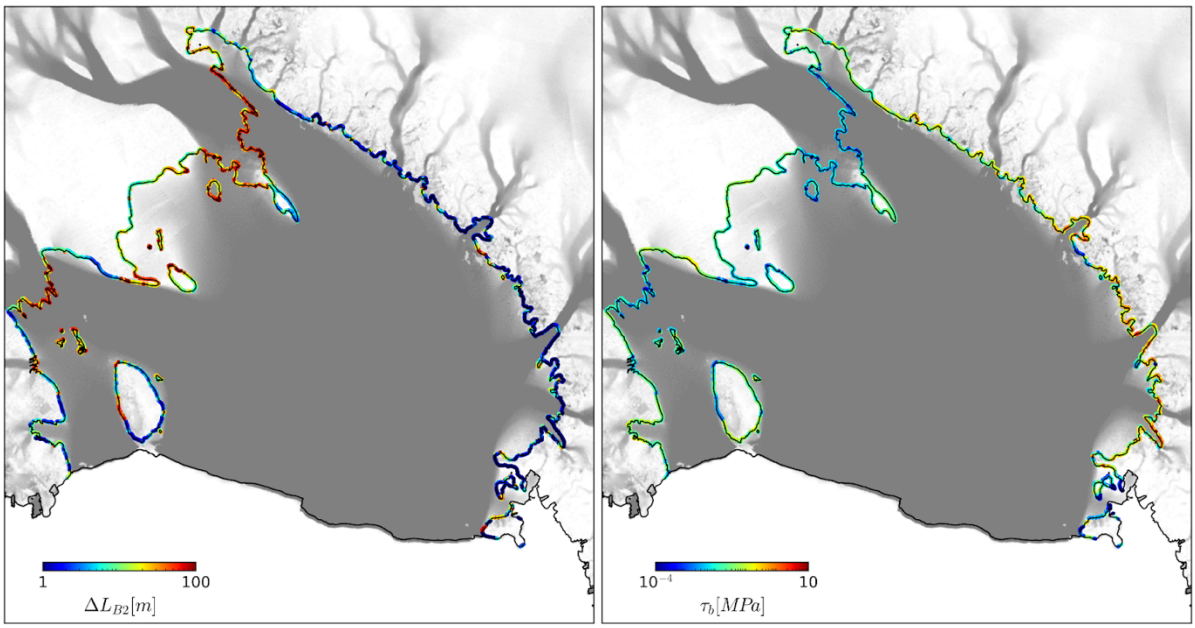

Figure S8. (a) Migration ΔL_{B2} of the grounding line for $\Delta SSH = 5 \times 10^{-2}$ m. (b) Basal shear stress τ_b at the grounding line averaged over the ensemble of simulation Ω_{15}.

References

Bromwich, D. H., Monaghan, A. J., Manning, K. W., and Powers, J. G.: Real-Time Forecasting for the Antarctic: An Evaluation of the Antarctic Mesoscale Prediction System (AMPS), Monthly Weather Review, 133, 579–603, https://doi.org/10.1175/MWR-2881.1, 2005.

Dee, D. P., Uppala, S. M., Simmons, A. J., Berrisford, P., Poli, P., Kobayashi, S., Andrae, U., Balmaseda, M. A., Balsamo, G., Bauer, P., Bechtold, P., Beljaars, A. C. M., van de Berg, L., Bidlot, J., Bormann, N., Delsol, C., Dragani, R., Fuentes, M., Geer, A. J., Haimberger, L., Healy, S. B., Hersbach, H., Hólm, E. V., Isaksen, L., Kållberg, P., Köhler, M., Matricardi, M., McNally, A. P., Monge-Sanz, B. M., Morcrette, J.-J., Park, B.-K., Peubey, C., de Rosnay, P., Tavolato, C., Thépaut, J.-N., and Vitart, F.: The ERA-Interim reanalysis: configuration and performance of the data assimilation system, Quarterly Journal of the Royal Meteorological Society, 137, 553–597, https://doi.org/10.1002/qj.828, 2011.

Fretwell, P., Pritchard, H. D., Vaughan, D. G., Bamber, J. L., Barrand, N. E., Bell, R., Bianchi, C., Bingham, R. G., Blankenship, D. D., Casassa, G., Catania, G., Callens, D., Conway, H., Cook, A. J., Corr, H. F. J., Damaske, D., Damm, V., Ferraccioli, F., Forsberg, R., Fujita, S., Gim, Y., Gogineni, P., Griggs, J. A., Hindmarsh, R. C. A., Holmlund, P., Holt, J. W., Jacobel, R. W., Jenkins, A., Jokat, W., Jordan, T., King, E. C., Kohler, J., Krabill, W., Riger-Kusk, M., Langley, K. A., Leitchenkov, G., Leuschen, C., Luyendyk, B. P., Matsuoka, K., Mouginot, J., Nitsche, F. O., Nogi, Y., Nost, O. A., Popov, S. V., Rignot, E., Rippin, D. M., Rivera, A., Roberts, J., Ross, N., Siegert, M. J., Smith, A. M., Steinhage, D., Studinger, M., Sun, B., Tinto, B. K., Welch, B. C., Wilson, D., Young, D. A., Xiangbin, C., and

Zirizzotti, A.: Bedmap2: improved ice bed, surface and thickness datasets for Antarctica, The Cryosphere, 7, 375–393, https://doi.org/10.5194/tc-7-375-2013, 2013.

Haidvogel, D. B., Arango, H., Budgell, W. P., Cornuelle, B. D., Curchitser, E., Di Lorenzo, E., Fennel, K., Geyer, W. R., Hermann, A. J., Lanerolle, L., Levin, J., McWilliams, J. C., Miller, A. J., Moore, A. M., Powell, T. M., Shchepetkin, A. F., Sherwood, C. R., Signell, R. P., Warner, J. C., and Wilkin, J.: Ocean forecasting in terrain-following coordinates: Formulation and skill assessment of the Regional Ocean Modeling System, Journal of Computational Physics, 227, 3595–3624, https://doi.org/10.1016/j.jcp.2007.06.016, 2008.

Kobayashi, S., Ota, Y., Harada, Y., Ebita, A., Moriya, M., Onoda, H., Onogi, K., Kamahori, H., Kobayashi, C., Endo, H., Miyaoka, 115 K., and Takahashi, K.: The JRA-55 Reanalysis: General Specifications and Basic Characteristics, J. Meteorol. Soc. Jpn. II, 93, 5–48, https://doi.org/10.2151/jmsj.2015-001, 2015.

Makinson, K., King, M. A., Nicholls, K. W., and Gudmundsson, G. H.: Diurnal and semidiurnal tide-induced lateral movement of Ronne Ice Shelf, Antarctica, Geophys. Res. Lett., 39, L10501, https://doi.org/10.1029/2012GL051636, 2012.

Menemenlis, D., Campin, J., Heimbach, P., Hill, C., Lee, T., Nguyen, A., Schodlok, M., and Zhang, H.: ECCO2: High Resolution Global Ocean and Sea Ice Data Synthesis, 2008, OS31C–1292, https://ui.adsabs.harvard.edu/abs/ 2008AGUFMOS31C1292M, 2008.

Morlighem, M., Rignot, E., Binder, T., Blankenship, D., Drews, R., Eagles, G., Eisen, O., Ferraccioli, F., Forsberg, R., Fretwell, P., Goel, V., Greenbaum, J. S., Gudmundsson, H., Guo, J., Helm, V., Hofstede, C., Howat, I., Humbert, A., Jokat, W., Karlsson, N. B., Lee, W. S., Matsuoka, K., Millan, R., Mouginot, J., Paden, J., Pattyn, F., Roberts, J., Rosier, S., Ruppel, A., Seroussi, H., Smith, E. C., Steinhage, D., Sun, B., Broeke, M. R. van den, Ommen, T. D. van, Wessem, M. van, and Young, D. A.: Deep glacial troughs and stabilizing ridges unveiled beneath the margins of the Antarctic ice sheet, Nat. Geosci., 13, 132–137, https://doi.org/10.1038/s41561-019-0510-8, 2020.

Orsi, A. H. and Wiederwohl, C. L.: A recount of Ross Sea waters, Deep Sea Research Part II: Topical Studies in Oceanography, 56, 778–795, https://doi.org/10.1016/j.dsr2.2008.10.033, 2009.

Rignot, E., Jacobs, S., Mouginot, J., and Scheuchl, B.: Ice- Shelf Melting Around Antarctica, Science, 341, 266–270, https://doi.org/10.1126/science.1235798, 2013.

Shchepetkin, A. F. and McWilliams, J. C.: The regional oceanic modeling system (ROMS): a split-explicit, free-surface, topography-following-coordinate oceanic model, Ocean Model., 9, 347–404, https://doi.org/10.1016/j.ocemod.2004.08.002, 2005